Research Article

Yuan Li* and Junhong Su

Optical and laser damage resistance: Role of periodic cylindrical surfaces

https://doi.org/10.1515/phys-2024-0119
received August 15, 2024; accepted December 16, 2024

Abstract: Traditional laser thin film optical components are specially designed layered structures made of two or more materials. However, as the number of layers increases, the anti-laser damage ability of the optical elements is significantly reduced. In this study, a single-layer structured surface is designed to have better optical transmittance than its homogeneous substrate. It also shows potential advantages in laser damage resistance applications. The transmittance and laser damage morphology of periodic cylindrical surfaces and their uniform substrates using a combination of experimental and simulation methods are examined. According to ISO21254, the laser-induced damage threshold (LIDT) of the structured surface and the uniform substrate were measured on a 1-on-1 irradiation of a 1,064 nm laser with a pulse width of 10 ns. The measured LIDT values were (15.3 ± 1.15) J/cm^2 for the structured surface and (15.2 ± 1.09) J/cm^2 for the uniform substrate. The damaged morphology of the structured surface was analyzed using a polarizing microscope to study its periodic distribution. Additionally, the electric field distribution on the surface of the structure and its uniform substrate was simulated using the finite element method. The results indicate that the damage characteristics of the structured surface are influenced by the surface structure, and the presence of the structure influences the energy distribution of laser deposition. This study serves as a valuable reference for further research into the laser damage mechanism of structured surfaces.

Keywords: laser-induced damage threshold, structured surface, optical elements, periodic columnar distribution, silicon dioxide

*** Corresponding author: Yuan Li,** School of Physics and Telecommunication Engineering, Shaanxi University of Technology, Han Zhong, China, e-mail: liyuan@snut.edu.cn, 173361788@qq.com
Junhong Su: School of Opto-electronical Engineering, Xi'an Technological University, Xi'an, China, e-mail: sujhong@126.com

1 Introduction

Laser damage to optical components is a major issue in high-power laser systems, significantly impacting the performance and reliability of these components [1,2]. Improved laser-damage-resistant materials are vital for industries dependent on high-power laser systems, such as medical imaging, industrial processing, energy production, and high-energy laser weapons. Enhancing resistance to laser-induced damage is key to advancing these sectors and ensuring the efficient operation of crucial laser systems. Traditionally, the laser damage resistance of optical components depends on laser thin films, typically created with multi-layer structures to provide specific optical properties such as anti-reflection, high reflection, polarization, and filtering. Generally, more layers increase the risk of damage. However, the anti-damage performance of these thin films has reached its limit, creating a bottleneck that fails to meet the growing demands of modern high-power laser systems. Improving the resistance of optical elements to laser damage has been a focus of extensive research, prompting the investigation of new surface structure technologies to reduce damage. The structural surface is a planar optical element that manipulates light through its structure, unlike multi-layer dielectric films. Structural surfaces have shown the ability to achieve flexible optical manipulation [3–6], offering advantages over traditional optical components [7–9] and holding potential for applications in high-power laser systems. Flexible optical manipulation refers to the ability to dynamically and precisely control the optical properties of light, including its amplitude, phase, polarization, wavelength, and propagation direction, at the deep-subwavelength scale. This level of control is unprecedented in conventional optics, which typically relies on light refraction and propagation.

However, for optical elements with micro/nanostructures on the surface, the influences of the structured surface on laser damage performance are more complex. The damage mechanism in nanosecond laser-induced optical dielectric materials arises from multiple factors. Key mechanisms include field damage (such as multi-photon absorption, avalanche ionization, and plasma formation), thermal effects (including thermal diffusion, phase changes, and stress or

strain in the material), nonlinear optical processes (such as two-photon absorption and self-focusing), and inherent material properties (such as dielectric constant, thermal conductivity, and mechanical strength) [10]. Surface defects [11,12] and electric field enhancement [13] at the surface also play significant roles in laser damage. Du *et al.* [14] utilized experimental and simulation techniques to investigate the periodic arrangement of cylindrical subwavelength gratings on a fused quartz substrate. The results indicate that the absorption center and nonuniform thermomechanical distribution on subwavelength gratings (SWGs) result in a lower laser-induced damage threshold (LIDT) on the columnar structured fused quartz compared to the bare fused quartz substrate. Ye *et al.* [15] utilized the finite-difference time-domain method to simulate the distribution of electric field in subwavelength gratings on a fused quartz substrate. The findings indicated a strong correlation between the electric field distribution (EFD) and the periodic surface structure, and the LIDT of SWG to be nearly as high as for plain bulk fused silica. The results are contrary.

Building on these foundational studies, our current work delves into the intricate relationship between micro/nanostructured surfaces and their laser damage resistance, offering novel insights that could significantly progress the development of high-power laser systems. Our previous studies [16–18] have indicated that the surface of nanostructures has a significant impact on laser response, potentially resulting in damage properties that differ from those of typical materials. Nevertheless, detailed research in this field is currently limited, particularly regarding comprehending the mechanism and nature of damage caused by a 1,064 nm laser.

Compared to metal-dielectric materials, dielectric materials generally have a higher resistance to laser damage [19–22]. Nasiri *et al.* studied the laser damage properties of all-medium and metal-medium mirrors and found that all-medium mirrors have a higher laser damage threshold [19]. Lin *et al.* studied the laser damage resistance of HfO_2/SiO_2 multilayer dielectric gratings and films and found that the LIDT of such multilayer dielectric gratings is lower than that of multilayer dielectric films. This is mainly caused by the grating's surface structure and the field enhancement of the incomplete clean surface [23].

As we know, silicon dioxide (SiO_2) is an ideal material for studying the effect of surface structure on laser damage properties. Silicon dioxide (SiO_2) is a widely used low-refractive index optical medium, which has the advantages of optical transparency, low absorption, low refractive index [24–27], dielectric properties, and structural adaptability, and is crucial in the design and manufacture of optical components. Its versatility improves the performance of other materials in optical applications and has strong resistance to laser damage [28,29]. Therefore, silicon dioxide (SiO_2) is an ideal material for studying the influence of surface structure on laser damage properties. Moreover, the structure of the silica surface can effectively adjust the refractive index [30], and customizable silica cylindrical grating can achieve a specific refractive index, which is necessary for subwavelength optical operation, giving it anti-reflection properties and potential advantages in resistance to laser damage.

This study investigates the laser damage resistance and transmittance of a columnar surface and its uniform substrate, which is quartz glass coated with a thin silicon oxide film. To further understand the effect of micro/nanostructure on laser damage, the influence of the SiO_2 material and its periodic cylindrical structure on the laser damage performance was compared. Numerical simulation analysis and experiments were used to study the effect of periodic columnar distribution on damage behavior under 1,064 nm laser irradiation. The results indicate that the damage mechanisms of the structured surface optical element caused by nanosecond pulse laser are complex. The results show that micro/nanostructured surfaces regulate the energy of laser deposition, leading to a complex damage mechanism attributed to the presence of the structure. The damage morphology is associated with the structure and periodic distribution of the optical elements. This study provides insights for designing and optimizing structural surface antilaser damage, enriching the strategy.

2 Materials and methods

2.1 Design and fabrication of sample

A structured surface with periodic columnar distributions and its homogeneous substrate were designed and fabricated for a comparative study of the laser damage resistance. Experimental studies indicate that 500 nm thick SiO_2 films exhibit greater resistance to laser damage compared to thicker films [16], which is crucial for our research on laser damage thresholds for grating structures. The homogeneous substrate consists of a 500 nm thick SiO_2 film on a 1 mm thick quartz glass base. Studying 500 nm high cylindrical feature gratings is essential for comparing and analyzing the laser damage resistance of homogeneous substrates, which is vital for achieving our research objectives and understanding the durability of structural surfaces against laser damage. To ensure the studies were comparable, the SiO_2 films were prepared from the same batch. The SiO_2

films were prepared by the plasma-enhanced chemical vapor deposition (PECVD) on quartz glass, which was from the same batch. Using SiH_4 and N_2O as reaction gases, the PECVD technique was used to fabricate a batch of SiO_2 films with the following deposition parameters: substrate temperature of 350°C, deposition pressure at 100 Pa, and gas flow rates of SiH_4 and N_2O at 20 sccm. The deposition rate was (15 ± 1) nm/min. These parameters were carefully selected based on preliminary experiments to optimize the properties of the SiO_2 thin film, including refractive index and extinction coefficient, which are crucial for LIDT applications. The measured refractive indices of SiO_2 film and quartz glass in the 700–2,500 nm band are 1.49 ± 0.02 and 1.45, respectively, which is in good agreement with the data published on the website [31].

Rigorous coupled wave analysis (RCWA) was employed to design the structure's surface parameters. This efficient and accurate semi-analytical technique transforms the partial differential equation of Fourier amplitudes into ordinary differential equations, enabling precise handling of complex media structures with minimal computational resources. Given the periodic nature of the studied structural surface, RCWA is particularly well suited for design and optimization. The design structure parameters of the sample are Λ = 1 μm, d = 500 nm, $f = d/\Lambda$ = 0.5, and h = 500 nm, respectively, where Λ is the period, d is the diameter, f is the duty cycle, and h is the column height. The scheme of the structured surface with periodic columnar distributions is shown in Figure 1, where Figure 1(a) is the side view and Figure 1(b) is the top view. The blue arrow in Figure 1(a) shows the laser incidence direction directly onto the structured surface.

The sample of this structural surface was fabricated by nanoimprint combined with ion beam etching, using the same preparation process as our previous work [16]. Please refer to our previous work for more detailed process flow. Nano-imprinting technology combines an inductively coupled plasma (ICP) and reactive ion etching (RIE) system to create a periodic cylindrical nanocolumn array on a substrate. The array has a height of 500 nm, a period of 1 μm, and a diameter of 500 nm, with the substrate being 1 mm thick quartz glass coated with a 500 nm SiO_2 film. During the nanoimprint process, maintaining the substrate temperature at 100°C and pressure at 2 bar prevents damage to the film, while a 60 s holding time allows the anti-reagent to flow and fill the mold. For the ICP-RIE etching process, the mixture of CF_4 and H_2 is conducive to controlling the etching rate and the formation of the passivation layer. The gas flow rate is 50 sccm for CF_4 and 5 sccm for H_2, and the etching rate is 100 nm/min. When the bias voltage is 150 V, it helps to increase the ion energy, thus increasing the etching rate and

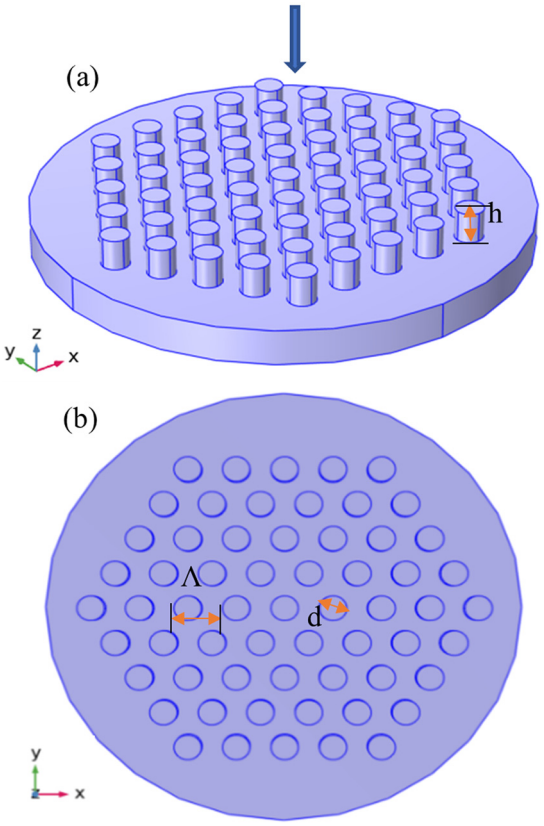

Figure 1: Scheme of the structured surface with periodic columnar distributions: (a) top view and (b) side view.

anisotropy. The prepared surface samples have good repeatability and stability. After these processes, the surfaces underwent ultrasonic cleaning in deionized water with a non-abrasive detergent at 40 kHz for 20 min to remove residual contaminants. This was followed by a thorough rinse in deionized water and a nitrogen purge for drying to prevent water spots.

The scanning electron microscope (SEM) diagram of the sample is shown in Figure 2. The structural parameters of the sample were measured multiple times to ensure accuracy and consistency. The mean values are Λ = 1.006 μm, d = 513 nm, and h = 498 nm, with standard deviations of Λ = 0.03 μm, d = 15 nm, and h = 10 nm, respectively. The coefficient of variation for each parameter is Λ = 3%, d = 3%, and h = 2%. These statistical measures indicate that the preparation error is within an acceptable range, demonstrating the high precision and quality of our fabrication process.

2.2 Optical characteristics

The transmittance spectra of samples were measured using a spectrophotometer (Lambda 950, Perkin Elmer Company,

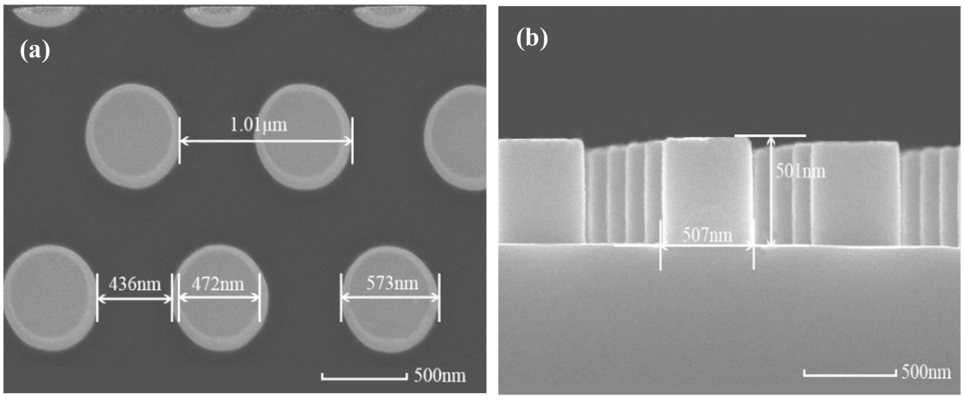

Figure 2: (a) Overhead and (b) cross-sectional SEM micrographs of nanostructured surface.

Waltham, MA, US). The spectral curves for the samples are displayed in Figure 3. Figure (a) shows the measured spectral curves and the simulated curves for the samples as a function of wavelength. Figure (b) is a magnified view of Figure (a). The transmittance can be presented more clearly. The blue unmarked and the black cross-curves represent the simulated and measured curves of the structural surface, while the green asterisk-marked and red triangle-marked curves correspond to the simulated and measured curves of the SiO_2 film, respectively.

From 1,250 to 2,400 nm, the average simulated and measured transmittance of the structural surface is 97.5 and 95.8%, and the average simulated and measured transmittance of the SiO_2 film with a thickness of 500 nm is 96.1 and 94.2%, respectively. Although the measured transmittance is almost 2% lower than the simulated transmittance, it is reasonable because the simulation only considered one surface and did not account for the reflection loss at the back and the interface of the samples.

In the range of 800 and 1,250 nm, the simulated transmittance of the structural surface oscillates due to the appearance of higher-order diffraction for the surface of the periodic distribution structure, where the period and wavelength satisfy the diffraction formula, as shown in formula (1) [32]. The measured transmittance curve is consistent with the average value of the simulated transmittance:

$$n_s \sin(\alpha) + n_0 \sin(\beta_m) = m\frac{\lambda}{\Lambda}, \quad (1)$$

where Λ, n_s, n_0, and λ represent the period of the structural surface, the refractive index of silica material and air, and the wavelength of light wave, respectively. α and β_m represent the incidence angle and the diffraction angle of the m-order diffraction order, respectively, where m is the

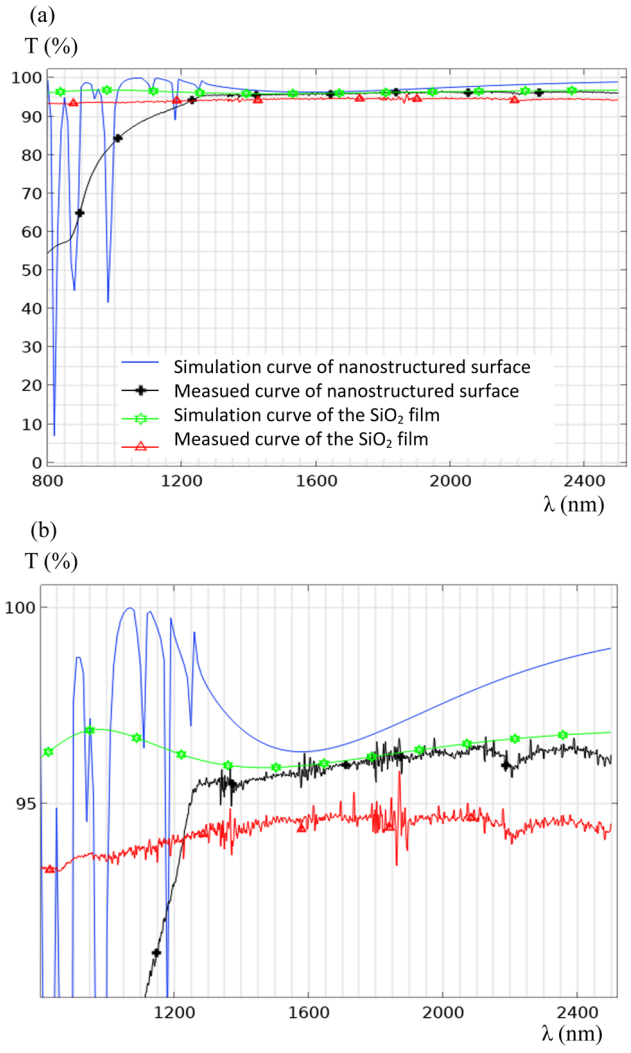

Figure 3: Transmittance of the samples: (a) comparison of measured and simulated transmittance spectra of the samples as a function of wavelength at normal incidence and (b) the partial enlarged view.

diffraction order. When $m = 0$, this is known as the reflection law. Without higher-order diffraction above order 2, formula (1) is further transformed into formula (2):

$$2\lambda > \Lambda(n_s|\sin(\alpha)| + n_0). \quad (2)$$

The refractive indices of silica and air are 1.49 and 1, respectively. The magnitude of a sine function is always less than or equal to 1. As shown in Eq. (2), for an average measured period of 1.01 µm, there is no high-order diffraction on the structural surfaces, and the incident wavelengths should be greater than 1,257 nm. It is not difficult to see that the simulated transmittance curve is in good agreement with the measured curve.

2.3 Experimental setup for testing laser-induced damage

According to the ISO21254-2 standard [33], the experimental setup schematic for testing the LIDT of samples is illustrated in Figure 4 [16]. The Nd: YAG laser beam is guided through the expanding system and subsequently focused into the attenuator. The attenuation is meticulously fine-tuned to achieve the desired laser energy output. To divide the beam into two separate paths, a spectroscope is employed. One of the split beams is measured by an energy meter, while the other is directed onto the sample surface *via* the lens. The energy meter reading is then used to determine the exact amount of laser energy applied to the sample surface. The laser operates at 1,064 nm with a pulse width of 10 ns. The light spot is Gaussian with a maximum energy of 400 mJ and a diameter of 0.8 mm.

The LIDT is a crucial parameter for assessing the laser damage resistance of optical components. According to the ISO21254 standard, a "1-on-1" zero-probability damage test method is used to determine the LIDTs for optical components in this study. Specific operations are as follows: this involves irradiating different points on the surface of a sample with a single pulse of specific energy. Each point is only irradiated once, and the number of damaged points is recorded. The imaging method is utilized to identify the damaged point, while CCD is used to capture images before and after laser irradiation to determine whether the point is damaged. The damage probability at each level is calculated as $p = m/k$, where m is the number of damaged points and k is the total number of irradiated points. The more energy levels measured, the closer to the true value, and the energy level should cover the damage probability range from 0 to 100%. Before the formal test, damage energy was predicted at the sample's edge to identify the maximum energy that does not cause damage and the minimum energy that does. The energy level is usually set to 10, ranging from 0 to 100%, and each level is tested at least 10 times. The horizontal axis represents the energy density, while the vertical axis represents the damage probability. Each dot illustrates the damage probability at a specific energy level. These points are fitted to a straight line using the least-squares method in Matlab. The intersection of this line with the horizontal axis indicates the energy density corresponding to a damage probability of zero, defined as the zero-probability laser damage threshold for the component.

3 Laser-induced damage test results

The LIDT test results for the samples are shown in Figure 5, where the blue dots depict the damage probabilities of the structural surface and the orange dots show the damage probabilities of the SiO_2 film at various fluence levels. The blue and orange lines correspond to fitting lines of the structural surface and SiO_2 film damage probabilities, respectively. The points where the lines intersect the

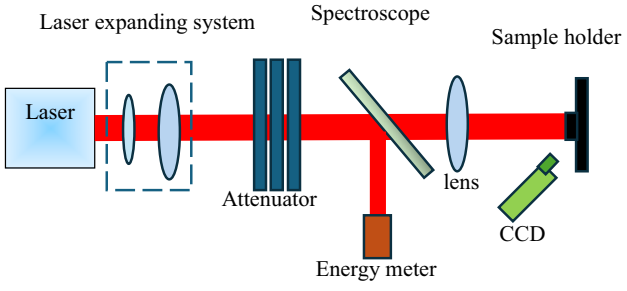

Figure 4: Scheme of the LIDT testing system for optical elements.

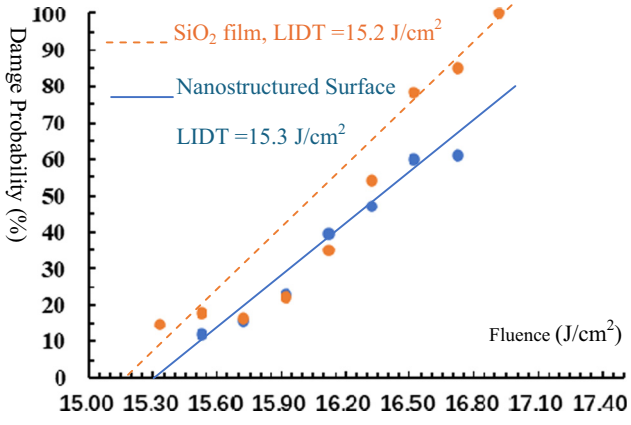

Figure 5: LIDTs of the samples.

y-axis reveal the energy density of the samples at which the damage probability is zero, known as the LIDTs of the samples. At a confidence level of 95%, it has been shown that the LIDT of the structural surface and the SiO_2 film are (15.3 ± 1.15) J/cm^2 and (15.2 ± 1.09) J/cm^2, respectively.

The data processing methods and details align with our previous work [34]. These measurements were taken in a controlled environment at 22 ± 1°C and 45 ± 5% relative humidity to ensure accuracy and reproducibility. It is demonstrated that the laser damage resistance of the structural surface is not decreased compared to the nonstructured SiO_2 film. Typically, as the number of layers increases, the LIDT decreases due to material mismatch, film absorption, interface defects, and other factors. The LIDT varies with the thickness of single-layer films [16]. In contrast to the LIDT values of 12.3 and 12.8 J/cm^2 (1,064 nm, 12 ns, 1-on-1) for traditional antireflection films [35], the structural surface shows promising advantages in light damage resistance.

Figure 6 shows a typical damage profile taken by a polarizing microscope (KEYENCE, VHX-7000, Japan). The pattern of damage is in the shape of a regular hexagon. The damage spot has a transverse size of 0.18 mm, which is smaller than the 0.8 mm diameter. It is not difficult to find that the typical damage morphology is related to the periodic cylindrical distribution pattern. This damage morphology is consistent in multiple test samples.

4 Discussions

To understand the formation mechanism of damage, the surface EFD of the structural surface and the homogeneous substrate (SiO_2 film with 500 nm thickness) was simulated by finite element method. The "elements" are numerically simulated using Floquet periodic boundary conditions based on the structure's periodic surface distribution characteristics. The triangular grid divides the geometric model, and near the structural elements is a denser grid that is one-tenth the size of the structural elements. We set the relative tolerance to 0.01 to address the convergence problem. The surface of the sample is vertically incident with a 1,064 nm pulsed laser. Figure 6 shows the EFD on the surface when the peak power of the laser incident is 1 W. The effect of surface EFD on laser damage was explored. TE and TM polarizations are fundamental modes that influence the EFD of the structured surface. Thus, simulating the EFD for the two modes on the structure's surface is essential. A lower electric field strength of the surface is beneficial to obtaining the optical device with a higher LIDT. Figure 7(a) shows the EFD diagram of the unstructured surface, while Figure 7(b) and (c) displays the EFD diagram of the structured surface with cylindrical periodic distribution for the TM and TE polarization incidents, respectively. The setup of coordinate axes is shown in Figure 7. The substrate plane is parallel to the XOY plane. When the magnetic field component Hy of the incident light is parallel to the *y*-axis, it is a TM wave; when the electric field component Ey of the incident light is parallel to the *y*-axis, it is a TE wave.

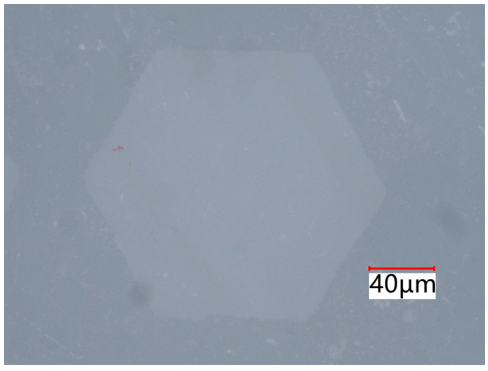

Figure 6: Damage morphology of the nanostructured surface.

From Figure 7, we can see that the electric field intensity on the film surface is higher than at the interface. The most intense electric field occurs at the interface between the column's base and the air, a pattern that remains consistent for both the TM and the TE waves. When the laser incident conditions are the same, the electric field intensity at the bottom of the cylinder and the air interface is higher than that on the surface of the film.

The inherent LIDT of the optical material is defined according to the plasma spark, as shown in Formula (3) [36], where c represents the speed of light; ε is the dielectric constant of the material; Time t_c is the time when the initial electron density in the conduction band rises to the critical electron density; and E denotes the electric field strength corresponding to the critical electron density of free electrons in the conduction band. According to the relation between the electric field intensity and LIDT, the intrinsic LIDT of the material is related to the electric field intensity at the critical electron density. This means that under the same laser incident conditions, the electric field intensity caused by the surface is lower compared to other surfaces, yet it exhibits a high resistance to laser damage.

$$D_{\text{th}} = \frac{1}{2} c\varepsilon \int_0^{t_c} E^2 \mathrm{d}t. \tag{3}$$

However, this was not the case. The LIDT of a material is influenced by both intrinsic and extrinsic factors. Intrinsic

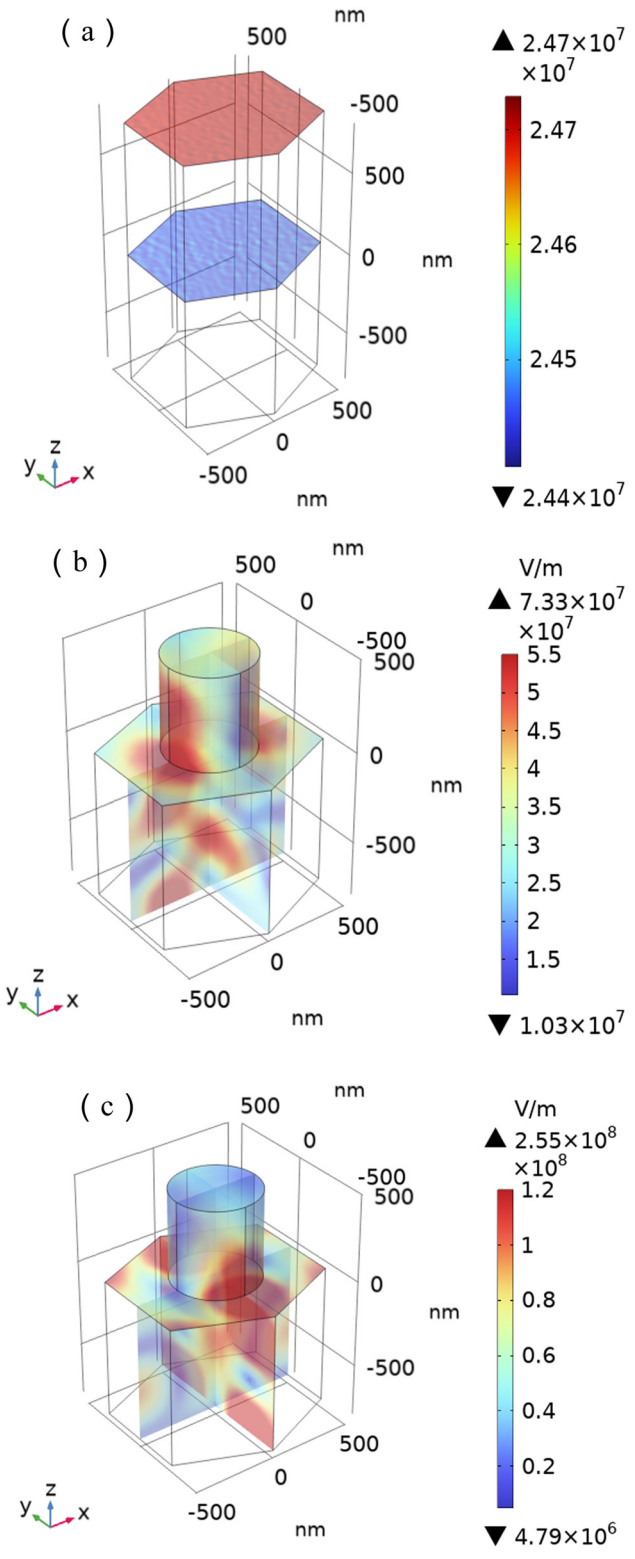

Figure 7: EFD on the surface of the samples: (a) EFD diagram of the unstructured surface, (b) EFD diagram of the structured surface with cylindrical periodic distribution for the TM wave, and (c) EFD diagram of the structured surface with cylindrical periodic distribution for the TE wave.

factors include linear and nonlinear absorption, as well as nonlinear phenomena such as self-focusing, stimulated Raman and Brillouin scattering, and electron avalanche breakdown. Extrinsic factors involve material defects, impurities, inclusions, and the quality of surface finishing. Despite structural differences, similar LIDT values can be observed due to the compensation of these factors. The physical mechanisms underlying LIDT values involve the interaction of the laser with the material, leading to the creation of defects and the subsequent propagation of these defects under the influence of the laser field. The boundary shape of the damaged appearance can rule out the defect as a cause. The structured surfaces in our study, despite their differences, may have similar defect densities or similar quality of surface finishing, which could contribute to similar LIDT values. The distribution of the electromagnetic field within the material is also crucial. The structured surfaces may couple differently with the incident laser, affecting the EFD. The surface that couples more energy from the laser will have a lower damage threshold due to higher field strength and energy density *via* constructive interference. However, if the structured surfaces are designed in such a way that they distribute the laser energy more evenly, they could exhibit similar LIDT values despite structural differences. Additionally, the electronic structure of the material plays a significant role in the observed damage threshold as a function of photon energy. Materials with similar electronic structures may require the same order of absorption process for electronic excitation, leading to similar LIDT values despite differences in structure.

In conclusion, the LIDT of a material is influenced by intrinsic and extrinsic factors. Intrinsic factors include linear and nonlinear absorption, as well as phenomena such as self-focusing, stimulated Raman and Brillouin scattering, and electron avalanche breakdown. Extrinsic factors encompass material defects, impurities, inclusions, and surface quality. Despite structural differences, similar LIDT values can arise from the compensation of these factors. The inherent LIDT of the material is usually much higher than the actual LIDT, and the actual material damage caused by the electric field may not be the only reason for the material damage.

For structural surfaces, laser-induced damage is not solely dictated by the surface electric field, *i.e.*, the LIDT of the structure surface is equivalent to that of its homogeneous substrate. This shows that the structure regulates the energy of the laser deposition and the damage mechanism is complicated due to the existence of the structured surface. The damage morphology suggests that the damage mode may be linked to a thermoelastic mechanism due to the periodic structure [37,38], although the specific damage process

requires further investigation. Future research should prioritize analyzing the thermal effects on the structural surface and conducting stress analyses. Additionally, studying the impact of nanosecond pulse duration on damage will enhance our understanding of laser-induced damage to the structural surface.

The findings on damage morphology and LIDT emphasize the importance of structural surface design. The antireflection effect is achieved through this structural design, allowing the desired optical transmittance to be attained with just one layer, unlike traditional optical films that require multiple layers. Furthermore, our analysis of the LIDT revealed that, unlike the typical trend of decreasing LIDT with more layers, our structured surface maintains a comparable or even superior LIDT compared to single-layer thin films. This signifies a significant advantage, suggesting that the structured design can enhance laser damage resistance without additional layers, making it particularly beneficial for applications where multilayer films are impractical or undesirable.

5 Conclusions

In this study, we have designed and characterized a single-layer surface with a cylindrical periodic structure, investigating its optical properties and resistance to laser-induced damage. Our findings reveal that within the spectral range of 1,250–2,400 nm, the transmittance of the cylindrical periodic structured surface exceeds that of its homogeneous counterpart. The LIDTs for the cylindrical periodic structure and the homogeneous substrate are determined to be (15.3 ± 1.15) J/cm^2 and (15.2 ± 1.09) J/cm^2, respectively. These findings indicate a negligible difference in their susceptibility to laser damage, suggesting that the periodic structure does not significantly impact the material's durability.

The finite element method simulated the surface EFD while excluding electric field enhancement as a direct factor in structured surface damage. The damage morphology of the structure indicates that the damage mode relates to the distribution of micro/nanostructures, and the arrangement of surface "units" influences laser energy deposition. These micro/nanostructures complicate the laser damage mechanism and impact overall laser damage performance. Further research is required to understand the specific damage process.

Acknowledgments: This research was funded by the National Natural Science Foundation of China (No. 61378050) and the University-Level Research Project of Shaanxi University of Technology (X20240026).

Funding information: This research was funded by the National Natural Science Foundation of China (No. 61378050) and the University-Level Research Project of Shaanxi University of Technology (X20240026).

Author contributions: All authors have accepted responsibility for the entire content of this manuscript and approved its submission.

Conflict of interest: The authors state no conflict of interest.

Data availability statement: The datasets generated and/or analyzed during the current study are available from the corresponding author on reasonable request.

References

[1] Moses EI, Lindl JD, Spaeth ML, Patterson RW, Sawicki RH, Atherton LJ, et al. Overview: Development of the national, ignition facility and the transition to a user facility for the ignition campaign and high energy density scientific research. Fusion Sci Technol. 2016;69(1):1–24.

[2] Manenkov AM. Fundamental mechanisms of laser-induced damage in optical materials: today's state of understanding and problems. Opt Eng. 2014;53(1):010901.

[3] Li X, Zhou Y, Ge S, Wang G, Li S, Liu Z, et al. Experimental demonstration of optical trapping and manipulation with multifunctional metasurface. Opt Lett. 2022;47:977–80.

[4] Zhang JH, Kivshar Y. Quantum metaphotonics: recent advances and perspective. APL Quantum. 2024;1(2):020902.

[5] Kuo HY, Vyas S, Chu CH, Chen MK, Shi X, Misawa H, et al. Cubic-phase metasurface for three-dimensional optical manipulation. Nanomaterials. 2021;11:1730.

[6] Xu Y, Su XR, Chai Z, Li JL. Metasurfaces toward optical manipulation technologies for quantum precision measurement. Laser Photonics Rev. 2024;18(3):2300355.

[7] Li YF, Zhang JH, Yang B. Antireflective surfaces based on biomimetic nanopillared arrays. Nano Today. 2010;5:117–27.

[8] Yang J, Yang J, Fu YG, Wu JS, Ouyang MZ, Dong LT, et al. Design and manufacturing of mid-infrared ultra-wide-angle antireflective composite micro-nano structure film. Opt Mater. 2024;149:115137.

[9] Chen YA, Sharan VN, Luo ZR, Chang CH. Enhancing optical transmission of multilayer composites using interfacial nanostructures. J Appl Phys. 2019;126(6):063101.

[10] Yang H, Cheng J, Liu ZC, Liu Q, Zhao LJ, Wang J, et al. Dynamic behavior modeling of laser-induced damage initiated by surface defects on KDP crystals under nanosecond laser irradiation. Sci Rep. 2020;10(1):500.

[11] Cheng XB, Wang ZS. Defect-related properties of optical coatings. Adv Opt Technol. 2014;3:65–90.

[12] Stolz CJ, Negres RA. Ten-year summary of the Boulder Damage Symposium annual thin film laser damage competition. Opt Eng. 2018;57:121910.

[13] Dong S, Jiao H, Wang Z, Zhang J, Cheng X. Interface and defects engineering for multilayer laser coatings. Prog Surf Sci. 2022;97(3):100663.
[14] Du Y, Wu X, Zhu MP, Le ZC. Theoretical and experimental research on laser-induced damage of cylindrical subwavelength grating. Opt Express. 2015;23(19):24296–307.
[15] Ye X, Huang J, Geng F, Liu HJ, Sun LX, Yan LH, et al. High power laser antireflection subwavelength grating on fused silica by colloidal lithography. J Phys D Appl Phys. 2016;49(26):265104.
[16] Li Y, Su JH, Xu JQ, Yang LH, Yang G. Optical and laser-induced damage characterization of porous structural silicon oxide film with hexagonal period by nanoimprint lithography. Coatings. 2022;12(3):351.
[17] Li Y, Su JH, Xu JQ, Yang G. Characterization of damage morphology of structural SiO_2 film induced by nanosecond pulsed laser. Open Phys. 2022;20(1):724–9.
[18] Li Y, Su JH, Xu JQ, Yang LH, Chen D, Yang GL. Polarization characteristics of the near-field distribution of one-dimensional subwavelength gratings. IEEE Access. 2021;9:24814–22.
[19] Zahra N, Hamidreza F, Morteza H, Mehdi M. Investigation of the laser induced damage thresholds of all-dielectric and metal-dielectric mirrors for a continuous wave at 10.6 μm. Opt Mater. 2021;114:110936.
[20] Jiao HF, Zhang JL. Research on damage mechanism and application of nanosecond laser coatings. Opt Precis Eng. 2022;30(21):2568–90.
[21] Han YX, Jin YX, Kong FY, Wang YL, Zhang YB, Cao HC, et al. High-repetition-rate and multi-pulse ultrashort laser damage of gold-coated photoresist grating. Appl Surf Sci. 2022;576:151819.
[22] Li Z, Xia Z. The damage mechanism and process of metal multilayer dielectric gratings induced by ps-pulsed laser. Appl Surf Sci. 2019;494(Nov.15):977–82.
[23] Lin XK, Zhao Y, Liu XF, Li D, Shuai K, Ma H, et al. Damage characteristics of pulse compression grating irradiated by a nanosecond laser. Opt Mater Express. 2022;12(2):643–52.
[24] Golosov DA, Vilya N, Zavadski SM, Melnikov SN, Avramchuk AV, Grekhov MM, et al. Influence of film thickness on the dielectric characteristics of hafnium oxide layers. Thin Solid Film. 2019;690:137517.
[25] Shawon A, Pallabi P, Vivek B, Paul S, Olaf S, Marcus T, et al. Heterostructure films of SiO_2 and HfO_2 for high power laser optics prepared by plasma-enhanced atomic layer deposition. Coatings. 2023;13(2):278–8.
[26] Gao L, Lemarchand F, Lequime M. Refractive index determination of SiO_2 layer in the UV/Vis/NIR range: Spectrophotometric reverse engineering on single and bi-layer designs. J Eur Opt Soc Rapid Publ. 2013;8:13010.
[27] Liu H. Atomic layer deposition for high power laser applications: Al_2O_3 and HfO_2. Phd dissertation, Leibniz University, Hannover, Germany; 2018.
[28] Congcong L, Yuan Z, Qing Z, Jinjin L, Wenhui C, Xueshen W, et al. Low-temperature deposition of high-quality SiO_2 films with a sloped sidewall profile for vertical step coverage. Coatings. 2022;12(10):1411.
[29] Mehrvar L, Drogoff BL, Menard M, Chaker M. TEOS-PECVD films for high-quality SiO_2 cladding layers in Si_3N_4-photonics with low mechanical stress and optical loss. 2024 Photonics North (PN). Vancouver, BC, Canada; 2024. p. 1–2.
[30] Wan LL, Yang J, Liu XR, Zhu JY, Xu G, Hao CC, et al. Enhanced antireflective and laser damage resistance of refractive-index gradient SiO_2 nanostructured films at 1064 nm. Pol J Chem Technol. 2024;26(2):25–30.
[31] RefractiveIndex.INFO website: © 2008-2022 Mikhail Polyanskiy [EB/OL]. [2008-2022] https://refractiveindex.info/?shelf=main&book=SiO2&page=Lemarchand.
[32] Lai M, Sridharan GM, Parish G, Bhattacharya S, Keating A. Multilayer porous silicon diffraction gratings operating in the infrared. Nanoscale Res Lett. 2012;7:645.
[33] Lasers and laser-related equipment. Test methods for laser-induced damage threshold. Standard ISO 21254:2011, International Organization for Standardization (2011).
[34] Li Y, Su J, Xu J, Yang L, Yang G. Fitting model of laser-induced damage threshold for optical elements with periodic surface. Laser Optoelectron Prog. 2022;59(23):2320001.
[35] Xu JQ, Su JH, Hui YX, Cheng YJ. Laser damage properties of 1064 nm anti-reflective films with different electric field distributions. J Optoelectron Laser. 2012;23(7):1268–73.
[36] Shang X, Zhang R, Ma P. Analysis of avalanche mechanisms in short-pulses laser-induced damage. Opt Laser Technol. 2010;42(1):234–46.
[37] Marin M, Hobiny A, Abbas I. The effects of fractional time derivatives in porothermoelastic materials using finite element method. Mathematics. 2021;9(14):1606.
[38] Sherief HH, El-Maghraby NM, Abbas MF. Two-dimensional axisymmetric thermoelastic problem for an infinite-space with a cylindrical heat source of a different material under Green–Lindsay theory. Mech Des Struct Mach. 2022;50(10):3404–16.